Chapter 8

Microfluidics for Soft Electronics

Babak Taghavi, Jiantong Li, Mikael Östling and Shi Cheng

Additional information is available at the end of the chapter

http://dx.doi.org/10.5772/63376

Abstract

Microfluidics- based soft electronic systems have the potential to assist conventional rigid devices and circuits to achieve extreme levels of elasticity in wearable electronics and other applications. The goal of employing microfluidics-based approach among other existing methods is to enhance users comfort through fulfillment of wearable's mechanical performance requirements such as flexibility, twistability, and stretchability. This chapter presents a brief survey of different solutions for developing elastic electronics and a thorough review of the progress in microfluidics-based approaches. This chapter mainly focuses on the description of the fabrication process, design, and measurement steps of different antennas and complex systems realized using microfluidic interconnects.

Keywords: Elastic antennas, liquid metal, microfluidics, stretchable electronics, wearable technology

1. Introduction

In recent years, wearable electronics have received increasing attention in both academic research and industrial development. Wearable electronics are being utilized in various applications, including healthcare and medical electronic devices [1] as well as consumer electronics and robotics [2]. Human body surfaces are huge compared to the sizes of electronic components. Large-area coverage is sometimes a must-have feature, where tiny wearable gadgets are certainly not a good fit. Consider an electronic system equipped with multiple sensors, each placed at a fingertip for pressure sensing, and a radio frequency (RF) transmitter associated with an antenna to wirelessly send out the sensing data. Each sensor is connected to the core transmitter circuit by long, in the order of 10 cm, interconnects. Additionally, an antenna with a size of few centimeters is needed for RF communication. Therefore, the overall size of such an integrated electronic device can be as large as 50 –100 cm^2. Using conventional rigid printed circuit board (PCB) techniques to develop this kind of systems would inevitably

lead to a clumsy gadget that will most likely give an uncomfortable experience to the wearer. As wearable devices intimately interact with users' body and skin, their physical shapes and impact on haptic feelings of wearers are very important design considerations. Human body is soft and our skin is stretchable, especially on joints, thus any external gadget that comes into seamless contact with our body should feature certain degree of flexibility and stretchability in order to facilitate natural motions [3]. Researchers have been experimenting different materials and assembly methods to create more human-friendly wearable systems. Flexibility can be achieved by implementing electronics on thin flexible substrates, ranging from polyimide- based Kapton films such as circuit boards to thin film transistors (TFTs) on device level. Such flexible electronic devices and systems can withstand moderate folding and twisting, but not stressing. Excessive straining often results in non-reversible mechanical deformation and permanent electrical failure. Achieving stretchability with maintained electronic functions is significantly more challenging. Radically new fabrication techniques and design strategies are required to realize soft electronics, capable of reaching extreme levels of reversible bendability, twistability, and stretchability.

Significant advances have been made in the emerging field of soft electronics in the past two decades. Great potential has been shown in numerous new appealing applications, e.g., body-worn healthcare/medical sensing systems, ergonomic units, and tissue engineering constructs, where conventional rigid, bulky electronics are facing insurmountable obstacles to fulfill the demands. One of the most promising concepts is soft, rubbery electronic devices, implemented in the form of elastic structures, materials, or a combination of both [4]. Wavy silicon ribbons to realize stretchable silicon integrated circuits (ICs) have been reported [5]. Also, integration of TFTs on prestressed substrates has been proposed [6].

Unlike complex, miniaturized semiconductor- based active circuits, many passive components such as interconnects, sensors, and antennas, which occupy the major areas in large-area electronic devices and systems, can only be shrunk at the expense of efficiency, sensitivity, and functionalities. Elasticity of such large passive devices, thereby, dominates the overall flexibility and stretchability of integrated electronics. Various approaches to implement stretchable interconnects have been presented [7,8]. One typical example is meandered metallic interconnects built on flex foils, operating at different frequency ranges [9]. Flexible and stretchable interconnects, realized by incorporating low melting temperature solder alloy into microstructured channels in polydimethylsiloxane (PDMS), were first proposed by Siegel, et al. [10]. Various properties of different solder metals and alloys, including melting temperature, electrical conductivity, Brinell hardness, and material costs, were also investigated. Later, room temperature liquid metal alloy-, eutectic gallium and indium (EGaIn), filled microfluidic channels acting as elastic direct current (DC) interconnects have been demonstrated [11]. Additional appealing characteristics of EGaIn, such as good rheological properties, excellent wetting on almost any surfaces, and low toxicity, make it well suited for microfluidics- based soft electronics that might be in proximity contact with human body in practical use [12]. The first stretchable electronic devices, operating at radio frequencies, are a liquid metal unbalanced loop antenna and a fluidic ultra-wideband planar inverted cone antenna (PICA). Both antennas were implemented by utilizing liquid metal alloy, galinstan,

incorporated into microstructured, elastomeric channel matrices [13,14]. Similar concept was also proposed to demonstrate a stretchable dipole antenna. Modified inhomogeneous elastomer substrate was subsequently used to significantly improve elasticity of stretchable antennas [15]. A hybrid integration approach for combining active circuits on flexible PCBs and large-area stretchable passive electronics for RF radiation sensing was later reported by Cheng and Wu [16]. This integration strategy was afterwards expanded to create multi-layer, self-contained, large-area, elastic wireless strain sensor [17]. Standalone patch antenna using serpentine channels filled with EGaIN was also published [18]. More recently, a reconfigurable fluidic serpentine antenna with varying resonant frequency in response to strain was presented [19]. Moreover, successful development of new fabrication techniques for microfluidics- based soft electronics has been demonstrated [20].

The following sections present and discuss recent advances in the emerging field of microfluidics -based soft electronics. This chapter focuses on ultracompliant, elastic electronic devices and systems, with the capability of wireless communications and remote sensing. Following sections start with an elaborate description of the fabrication process, followed by presentation of several application examples of microfluidics- based RF elastic electronics. Measurement results on foldable, twistable, stretchable antennas and integrated devices under different mechanical deformations are also shown. This chapter ends with a glimpse of some ongoing research activities at the Department of Integrated Devices and Circuits, KTH Royal Institute of Technology, Sweden, among which new advanced processing techniques and nanomaterials, e.g., inkjet-printed, high precision, graphene resistors and conductors, are being investigated to enable novel sensing functions. Furthermore, feasibilities of utilizing elastic, microfluidic RF energy harvesters for wireless charging of soft energy storage units or remote powering active stretchable electronics are discussed.

2. Fabrication process

Microfluidic channel design procedure can be concisely described in three major steps, which are soft lithography, reverse molding, and liquid metal injection. Similar to PCB routings, depending on the complexity and architecture of circuits and antennas, a single or a multi-layer configuration can be selected to develop an electronic system. First, fabrication processes of single-layer liquid metal- filled channel matrices embedded in PDMS elastomers are presented in this section. Subsequently, processing steps for implementing multi-layer microfluidics-based soft electronic devices are described in detail. Finally, heterogeneous integration method for connecting active circuits assembled on flexible PCBs to microstructured fluidic channels encased in elastomeric substrates is discussed.

2.1. Single-layer microfluidic, elastic channels

Single- layer microfluidic channels are developed on bare silicon wafers, which are used as the substrate for molding and formation of elastic layers. SU8 photoresist is employed as a reverse mold for fluidic channels, and its thickness determines the height of microfluidic

channels. SU8 photoresist is spin coated on a silicon wafer as shown in Figure 1(a). As discussed in the Introduction, microfluidic channels act the same as conductor traces on conventional PCBs; therefore, their patterns are designed in the similar way as routing the traces on PCBs. The designed patterns are then used to build the corresponding lithography mask. After transferring the pattern to the photoresist and removing unexposed parts, the mold is ready for casting the channels. Cross- sectional view of the developed mold on silicon is displayed in Figure 1(b). The prepared mold is then thermally stabilized at 150 °C for 30 minutes to enhance the adhesion between silicon and the remaining SU8 layer. PDMS is used as the soft substrate because of its stretchability, transparency, and relatively easy preparation process. PDMS is widely used in bioelectronics and microfluidic applications such as lab-on-a-chip. It is prepared by mixing PDMS prepolymer and cross linker (Elastosil RT601A and B, Wacker Chemie, Munich, Germany) with 9:1 mass ratio. As shown in Figure 1(c), PDMS should be poured on top of the silicon to form the substrate. In addition to the patterned structures, a thin layer of PDMS is prepared on the blank silicon wafer to form a cover layer for the reversely molded PDMS. After degassing, both patterned and blank PDMS layers are cured at 70 °C for 30 minutes to solidify the PDMS layers. Once the PDMS layers are ready, it is time to peel them off from the silicon carriers as illustrated in Figure 1(e). Before proceeding to the next step, numerous openings should be punched on the patterned structure so that the channels can be accessed for liquid metal injection through those openings. The PDMS layers are bonded together using corona discharging (ETP, Chicago, IL, USA) activation afterwards. At this stage, fabrication of the microfluidic channels is completed and the subsequent step is to inject galinstan into the channels as seen in Figure 1(g). Galinstan is a liquid metal alloy, consisting of 68.5%, Ga; 21.5%, In; and 10%, Sn. It is in liquid state from –19 to 1300 °C, and it also features a good electrical conductivity of 3.46×10^6 S/m and non-toxicity in comparison with mercury. Its excellent wettability on almost any surface simplifies the channel filling process and ensures good electrical continuity despite of mechanical deformation. After filling the channels, a visual inspection or a simple electrical conductivity check should be performed to ensure that all electrical connections are established as expected. All openings except feeding points for electrical measurement and interconnections with active circuits are sealed with uncured PDMS droplets to prevent any liquid metal leakage. Cross- sectional and top view of the resulting single-layer microfluidic channels filled with liquid metal in a PDMS substrate are shown in Figure 1(h) and (i).

2.2. Multi-layer microfluidic, elastic channels

Some applications necessitate multi-layer structures. Additional channel layers make it possible to implement more sophisticated structures that are not feasible to build in a single-layer configuration. As depicted in Figure 2, fabrication steps resemble the previously presented processes for constructing a single-layer structure. Extra channel layers, however, require more lithography and bonding steps. In most applications, as shown in Section 2.3, feeding points on the same side of an elastomer substrate are often needed to facilitate circuit assembly or characterizations. For assessing the bottom liquid metal filled channels from the top surface of the PDMS substrate, an additional inlet is punched through the top and middle layers after bonding. In the liquid metal injection phase, top layer channels are filled and then

http://dx.doi.org/10.5772/63376

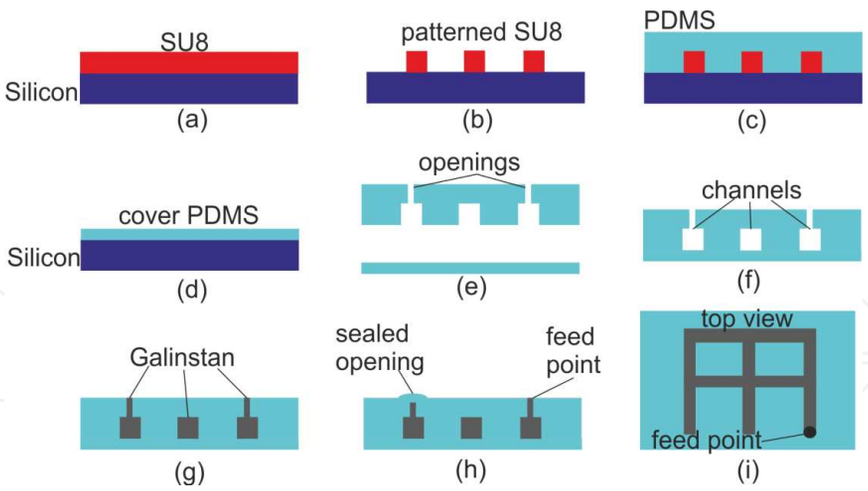

Figure 1. Single-layer microfluidic soft electronics fabrication process.

openings 2 and 5 are temporarily sealed by small pieces of Scotch tapes and opening 1 is encapsulated with uncured PDMS. Afterwards, the structure is flipped to the other side and galinstan is injected into the channel and both openings 3 and 4 are permanently sealed with uncured PDMS droplets. Later, the bonded substrate is flipped over and the temporary sealants are removed. After verifying all connections, the sample is cured at 85 °C for about 30 minutes.

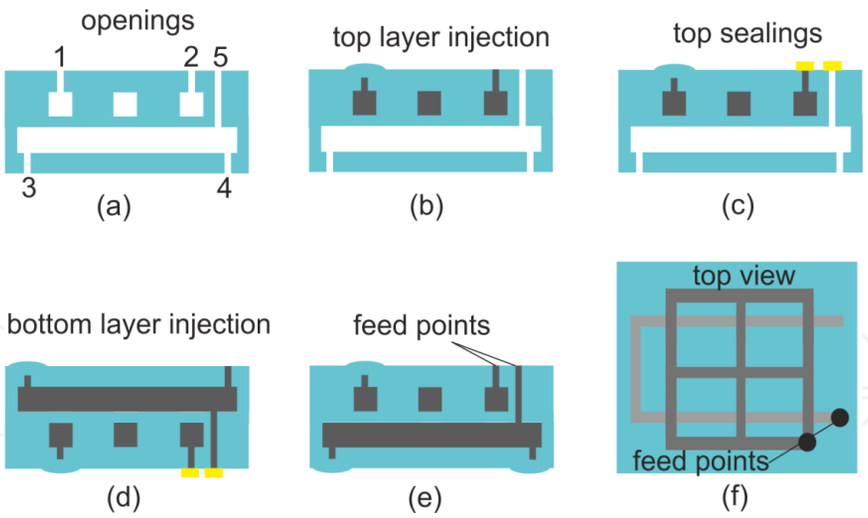

Figure 2. Processing steps of multi-layer microfluidic soft electronics.

2.3. Strain isolation cells

Active circuits play an essential role in modern electronic systems. Purely passive microfluidic soft electronics without any active components can only be used in very limited application scenarios in practice. A pressing issue is how to realize active electronics in bendable, flexible,

and stretchable manners. Implementing active circuits using microfluidic technologies would be ideal, but to our best knowledge, none of the existing microfluidic techniques support fabrication of high performance, basic active components, such as diodes and transistors, operating at gigahertz frequency range. A compromising solution is to heterogeneously integrate off-the-shelf packaged IC chipsets with passive microfluidic electronics. Here the biggest challenge lies in how to create reliable interconnections between rigid IC chips associated with discrete components and liquid metal filled elastic channels. Figure 3 illustrates a hybrid integration strategy, where IC chipsets as well as external lumped components are first assembled on a small piece of flexible PCB. Such a quasi-flexible circuit contains complex routing and most connections with high reliability. The subsequent step is to implement interconnects between flexible circuits and microfluidic elastic channels via solid metallic pins. Since much fewer connections are needed at this step, the overall reliability of such interconnects are dramatically improved. In order to address the issue of mechanical mismatch between elastomers and rigid components, strain isolation cells, the so-called local stiffening cells (LSCs), are introduced to encapsulate PCBs and metal pins with locally thickened PDMS. Although such cells are a bit more rigid than any other areas on the PDMS elastomer and inevitably degrade the overall elasticity of integrated devices to some extent, they can effectively minimize mechanical deformation around active circuits and interconnect pins when the entire devices are being folded, twisted, or stressed. Reliable galvanic contacts between metal pins and liquid metal alloy are crucial. Soldering tin plating on metallic pins is employed to ensure good electrical connections between solid and liquid metals, thanks to superior wetting properties of galinstan on tin. As depicted in Figure 3, a semi-spherical solder ball is also mounted on the bottom surface of each tin plated pin at one end to further improve the reliability of the connection to fluid metal.

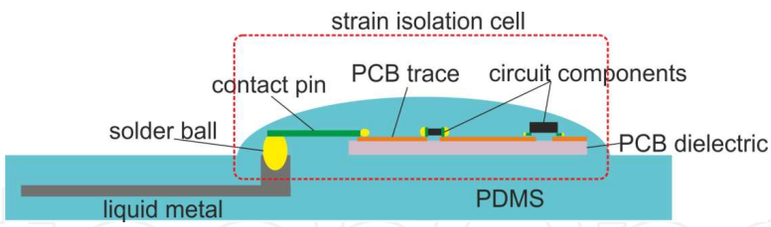

Figure 3. Hybrid integration of flexible active circuits and fluidic, elastic passive electronics.

3. Microfluidics- based elastic antennas and heterogeneously integrated RF electronics

Fabrication methods introduced in Section 2 are applied to realize different elastic RF-integrated electronic devices and systems. This section presents the design, fabrication, and measured results on standalone single-layer foldable, twistable, stretchable antennas; a fluidic soft RF radiation sensor; and a multi-layer, microfluidic, reversibly stretchable, large-area wireless strain sensor.

3.1. Liquid metal stretchable unbalanced loop antenna

An unbalanced loop antenna, operating at 2.4 GHz Industrial, Scientific, and Medical (ISM) band, is designed, fabricated, and characterized, using single-layer microfluidic channels filled with liquid metal. Schematic of the resulting loop antenna prototype as well as a cross-sectional view of microfluidic channels are shown in Figure 4. The antenna consists of a loop radiating element and a semi-circular, meshed ground plane. The loop is grounded at one end and isolated from the ground plane at the other end for coaxial cable feeding.

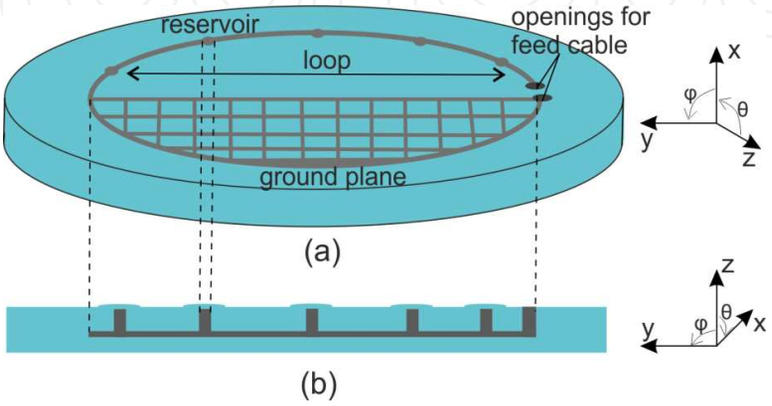

Figure 4. Schematic of liquid metal stretchable unbalanced loop antenna: (a) overlook view, (b) cross- sectional view.

The resonant frequency (f_{res}) of a loop antenna is a function of the loop length and can be approximated by the following Equation 1:

$$f_{res} \approx \frac{c}{2L_{loop}\sqrt{\varepsilon_{eff}}}, \quad (1)$$

where c is the velocity of light in free space, L_{loop} is the loop length, and ε_{eff} is the effective permittivity, which is about 1 for very thin PDMS layers. According to the equation, to obtain f_{res} = 2.4 GHz, the loop should be 5.6 cm in length. Numerical simulations are performed in Ansoft HFSS to verify antenna port impedance and radiation characteristics. As seen in Figure 4, numerous small cylinders are aligned along the loop-shaped channel, in which extra liquid metal alloy can be stored and released to guarantee reliable galvanic connections while the antenna is mechanically deformed. It should be noted that the presence of such liquid metal reservoirs results in slightly increased electrical length of the loop antenna so that a minor decrease in resonant frequency compared with the value calculated from the equation can be observed both in simulations and measurements. For example, if the loop length, L_{loop}, equals 56.4 mm, the resonant frequency, f_{res}, derived according to the equation should be 2.7 GHz. However, considering the effect of reservoirs, f_{res} = 2.4 GHz is obtained in numerical simulations. Once the simulation results meet the requirements, the antenna layout is exported to print a mask on transparency for subsequent soft lithography process. The printed plastic mask is then used to transfer the antenna patterns to the SU8 photoresist and to fabricate the antenna

following the fabrication steps described in Section 2.1. The resulting unbalanced loop antenna prototype is illustrated in Figure 5.

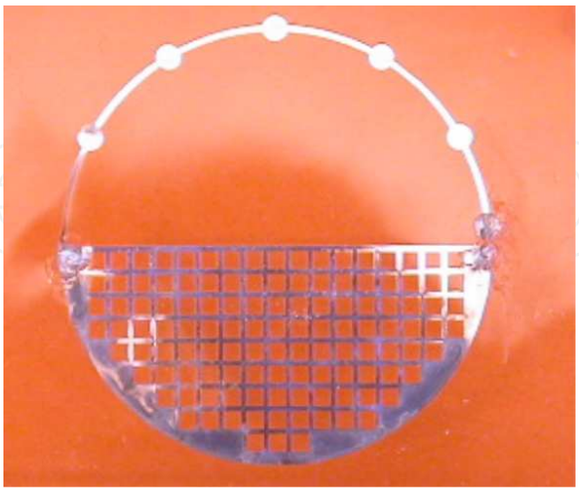

Figure 5. Photograph of the fabricated fluidic stretchable loop antenna.

In order to verify simulated results, the port impedance and radiation characteristics are measured using a vector network analyzer in an anechoic chamber. All experiments are first carried out with the antenna in its relaxed state. Measurement results along with the corresponding simulations are shown in Figure 6.

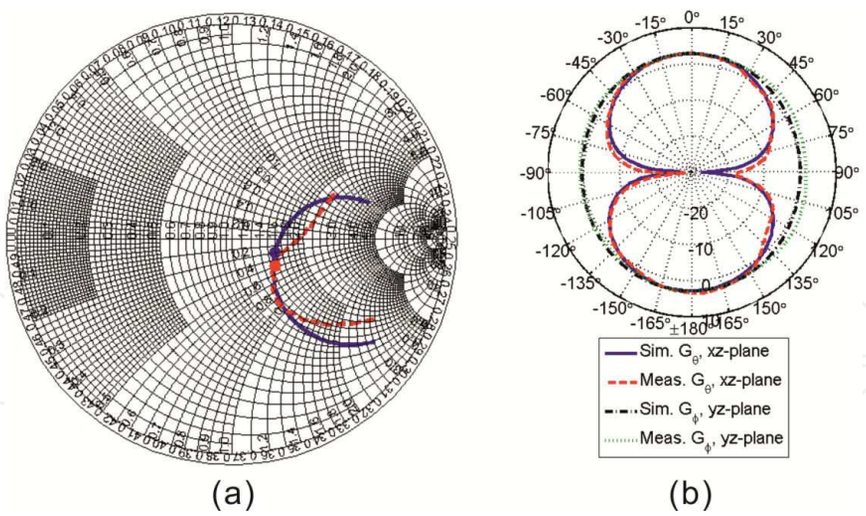

Figure 6. (a) Simulated (solid line) and measured (dotted line) reflection coefficient (S11) and (b) radiation patterns of the liquid metal- based stretchable unbalanced loop antenna. The coordinate system is depicted in Figure 4.

Mechanical performance of the microfluidic elastic antenna is tested under various deformations as shown in Figure 7. It is observed that the unbalanced loop antenna prototype can withstand omnidirectional straining, as well as severe folding and twisting, and return to its original shape after the removal of external forces.

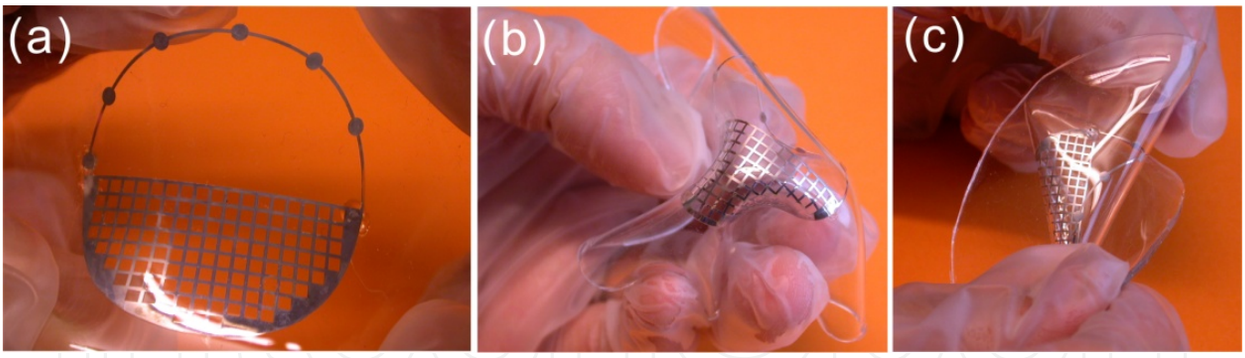

Figure 7. Photographs of the unbalanced loop antenna in (a) omnidirectionally strained, (b) twisted, and (c) folded states.

Electrical properties of the fluidic soft antenna in response to varying strains applied along its x- and y-axis are also characterized. Photographs of the elastic antenna in its relaxed and stressed states are displayed in Figure 8.

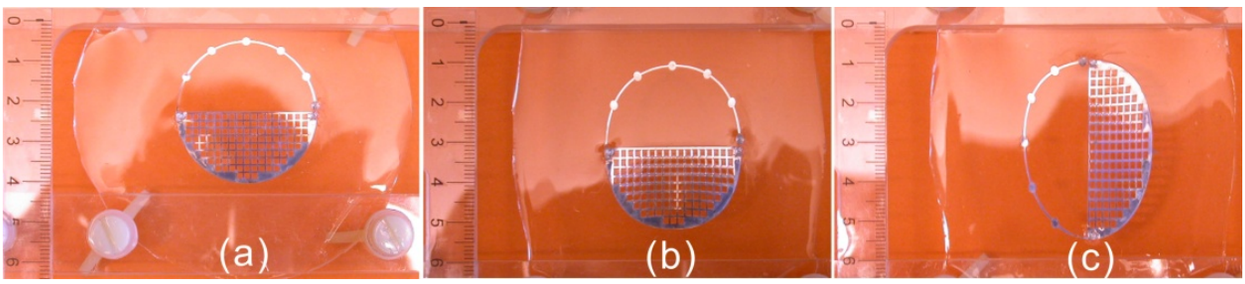

Figure 8. Photograph of the resulting elastic loop antenna in its (a) relaxed state, and with 40% stain along (b) x- and (c) y-axes. The corresponding coordinate system is shown in Figure 4.

Figure 9 presents measured port impedance and radiation patterns of the loop antenna in different states. The decrease in the antenna resonant frequency can be explained by an increased antenna size as a result of stretching. Antennas often exhibit wider radiation bandwidth than impedance bandwidth. This is why, measured radiation efficiency remains relatively stable despite being strained. No dramatic electrical performance degradation is detected in the experiments. It implies that no interruption in electrical connections occurs during antenna deformation. This is mainly because of the superior wettability of galinstan on the inner surfaces of elastomeric channels as well as its good electrical conductivity.

3.2. Elastic electromagnetic radiation sensor

Our daily life has been greatly benefiting from revolutionary mobile communication technologies rapidly developed in the past decades. Billions of portable devices, equipped with wireless links, are new parts of our everyday life. People and electronic equipment and systems are connected anywhere at any time. Rising concerns on potential health issues caused by the exposure to RF radiation has been expressed by both scientists and the public. It is, thereby, worth monitoring the level of ambient electromagnetic (EM) wave radiation to assess possible

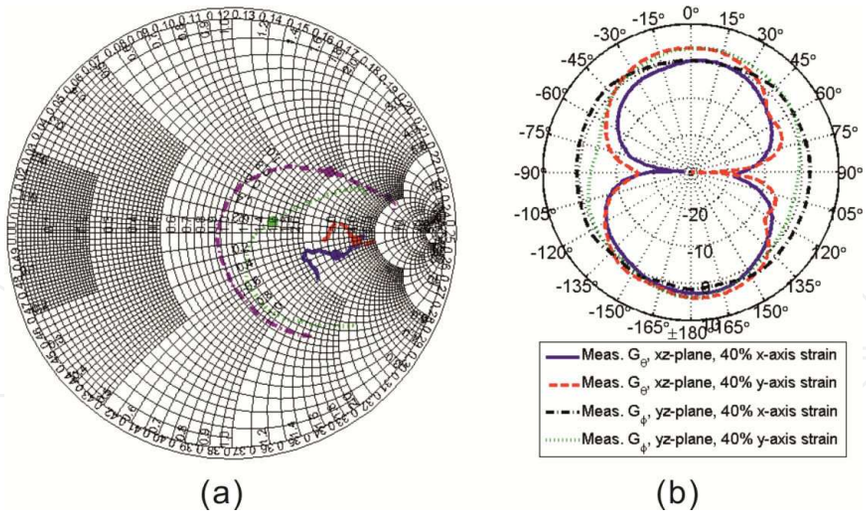

Figure 9. Measured (a) port impedance and (b) radiation patterns of the stretchable unbalanced loop antenna. The coordinate system is seen in Figure 4.

hazards and improve signal coverage quality in real life. In order to make it more portable, an EM radiation sensor can be developed as a wearable device. As discussed in the Introduction Section 1, better user experience can be achieved by constructing such a radiation sensor in ultracompliant, soft, and elastic manners. An RF power detector circuit assembled on a flex foil and encapsulated in an LSC is designed and interconnected to a microfluidics- based stretchable antenna to form a hybrid device, *cf.* Figure 10. Target operating frequency of the proposed radiation sensor is 900 MHz. A uniplanar rectangular unbalanced loop antenna is chosen for its ease of fabrication. The overall dimensions of the loop obtained from full wave simulations conducted in Ansoft HFSS are 86.9 mm × 88.0 mm × 1.0 mm. Ambient RF radiation is picked up from free space and directed to the input of the RF power sensing module via an elastic, fluidic antenna. The injected RF energy is then proportionally converted to DC voltages at the RF power detector IC output. The upper and lower sensing range of RF radiation energy is determined by the dynamic range of the power detection IC chipset. The chosen IC chip features a dynamic range from approximately –60 dBm to 0 dBm that is sufficient in most application scenarios. Apart from the core IC, three coupling and decoupling surface mounted device (SMD) capacitors along with an input matching inductor are needed. The entire power sensing active circuit mounted on a flexible PCB is powered externally, using a pack of four AA batteries connected serially. A light emitting diode (LED) is soldered at the voltage output of the power detector for visualization, which will be switched on when the received RF energy exceeds the pre-defined threshold. More details about the integrated RF radiation sensor can be found in Figure 10.

Prior to connecting the microfluidic antenna to the active circuit, electrical performance of both the antenna and the detector circuit is evaluated separately. Figure 11 shows measured reflection coefficient of the loop antenna in different stretched modes.

The output DC voltage of the standalone active circuit in response to varying RF input power is characterized. In this experiment, continuous wave (CW) signal with incremental power

http://dx.doi.org/10.5772/63376

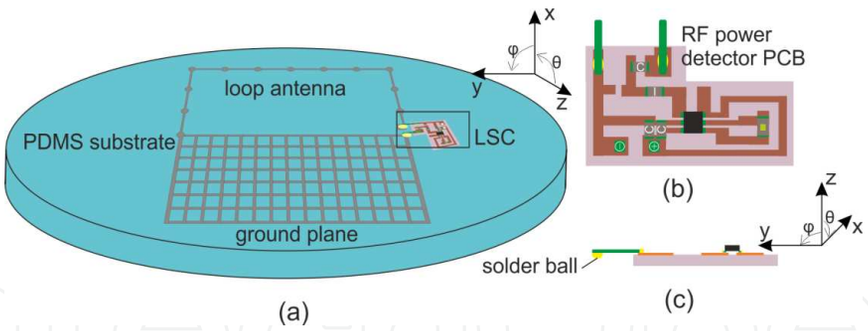

Figure 10. Schematic view of the elastic EM sensor: (a) overlook view of the integrated sensor, (b) top view, and (c) cross view of the flexible active circuit.

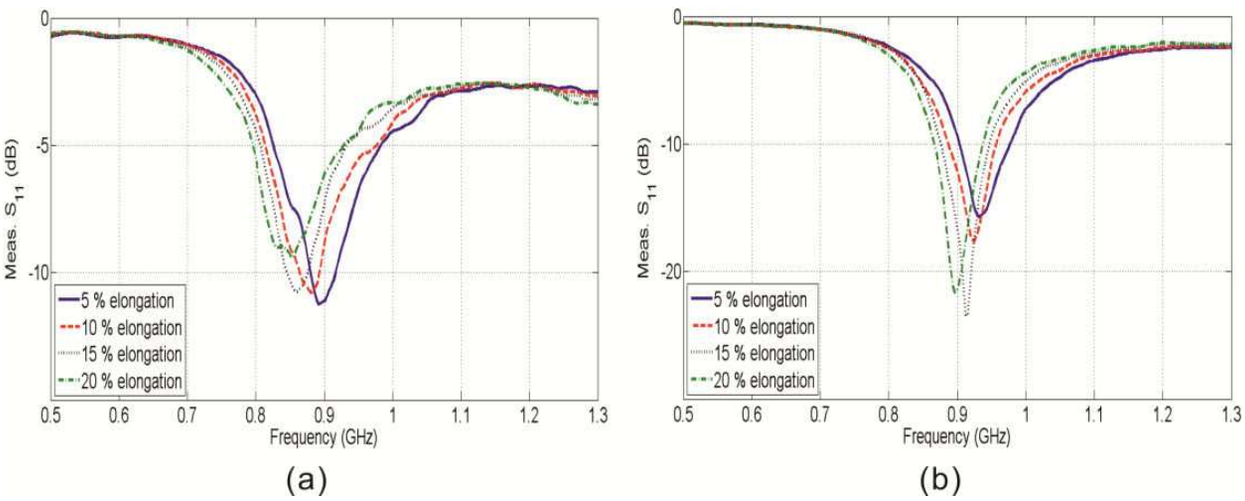

Figure 11. Measured reflection coefficient of the microfluidic elastic rectangular loop antenna in response to varying strain applied along its (a) *x*- and (b) *y*-axis. The coordinate system is presented in Figure 10.

level generated from a signal synthesizer is fed into the RF power detector input through an RF coaxial cable, and the LED indicator at the DC voltage output is temporally disconnected. The output voltage of the RF power detector as a function of input power is shown in Figure 12, in which fairly linear behavior is achieved over the entire dynamic range.

Subsequently, the PCB is assembled on the PDMS substrate using the proposed hybrid integration method. The fabricated elastic EM radiation sensor is shown in Figure 13.

The measurement setup illustrated in Figure 14 is utilized to demonstrate RF radiation sensing capability of the integrated sensor device in ordinary office environment. The distance from the dedicated radiation source comprising a standard horn antenna and a signal generator to the elastic RF radiation sensor is approximately 5 m.

The transmitter sends out a CW signal at 900 MHz with variable power levels into the free space. The LED indicator on the integrated stretchable sensor device is on when being exposed to high levels of radiation. The ON/OFF state of the LED indicator only depends on the level of the RF power received by the microfluidic stretchable loop antenna. Increased distance

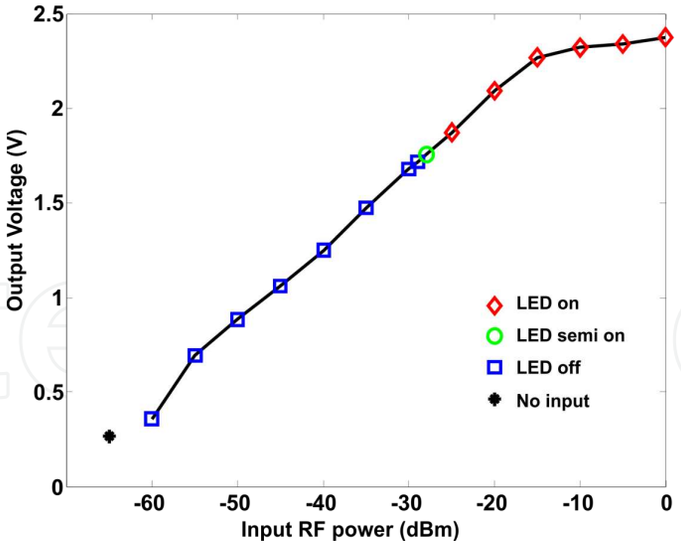

Figure 12. RF power module output voltage and LED status versus input RF power.

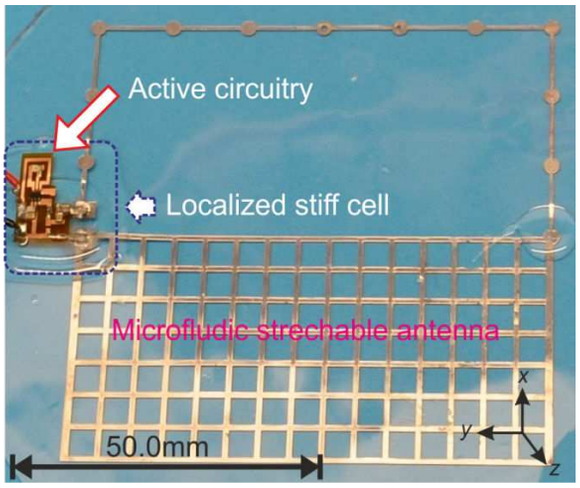

Figure 13. Photograph of the resulting elastic EM radiation sensor prototype.

between the radiation source and the sensor would result in greater free space loss. Higher power is, therefore, required from the RF signal generator to turn on the LED in this case. In addition to measurements in its relaxed state, the stretchable EM radiation detector is also tested in its folded, twisted, and strained modes. Figure 15 shows that the implemented microfluidics- based soft radiation sensor prototype remains functioning regardless of deformation.

3.3. Fluidic, elastic ultra-wideband antenna

Antennas with broad operational frequency bands are sometimes required. In ultra-wideband (UWB) systems, an extremely broad frequency range from 3.1 GHz to 10.6 GHz needs to be covered using a single antenna. Implementing a UWB antenna in highly flexible, bendable,

http://dx.doi.org/10.5772/63376

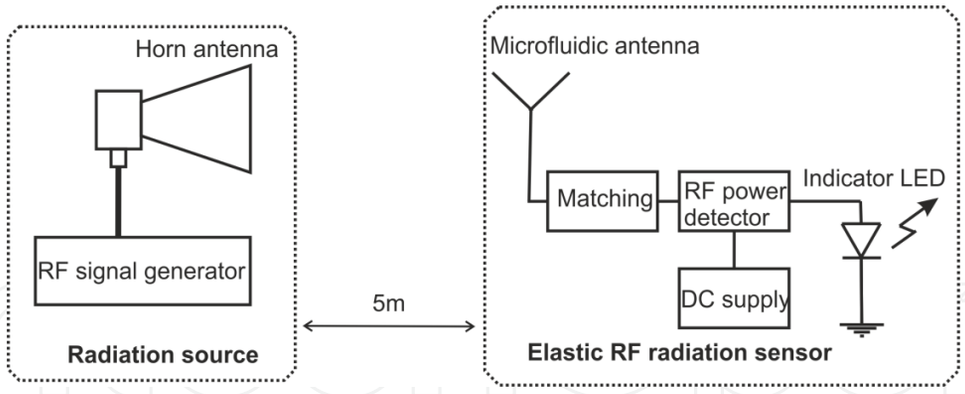

Figure 14. Schematic of the demonstration setup for the implemented elastic RF radiation sensor.

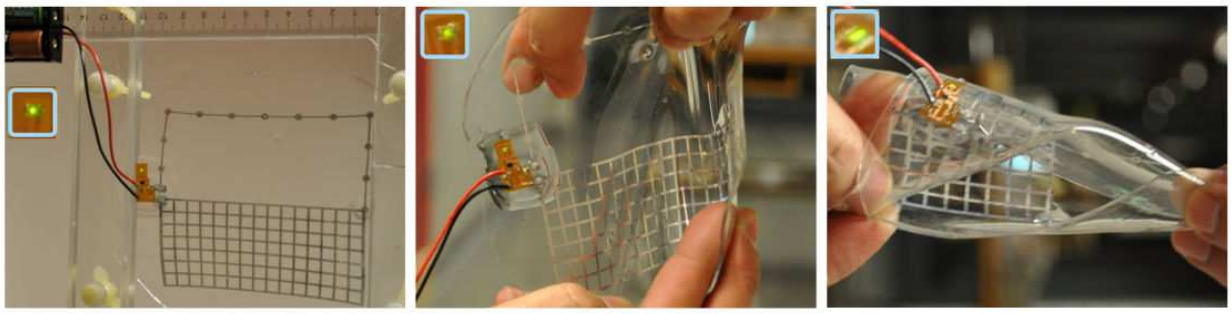

Figure 15. Photographs of the elastic EM radiation sensor operating under deformation: with 15% elongation along its (a) *x*- and (b) *y*-axis, (c) omnidirectional stressing, and (d) severe twisting. The corresponding coordinate system can be found in Figure 10.

and stretchable formats would be of great interest. Such an antenna can also be deployed in other applications that only require a fractional bandwidth of UWB, as it is expected to feature robust electrical characteristics in some narrower frequency ranges under deformation. A non-resonant antenna, PICA, is chosen because of its uniplanar configuration and ease of fabrication. The lower and upper operational frequencies of a PICA are determined by the height of the inverted cone and the size of the gap between the radiator and the ground, respectively. Its tapered shape gradually transforms the free space impedance of 377 Ω to 50 Ω over a wide frequency range. Full wave simulations performed in Ansoft HFSS suggest a radius of 10 mm (R) and a gap size of 300 μm (G) for covering the operational frequency range of 3–11 GHz. Schematic views of the liquid metal elastic PICA are seen in Figure 16. Similar to the previously presented microfluidic antennas, its ground and radiating element are realized in meshed configurations to separate the top and bottom PDMS membranes.

Mechanical properties of the fabricated antenna are first evaluated. Figure 17 shows that the resulting PICA prototype is reversibly stretchable, foldable, and twistable. After removing external forces, the antenna always returns to its original shape without any visible mechanical damages.

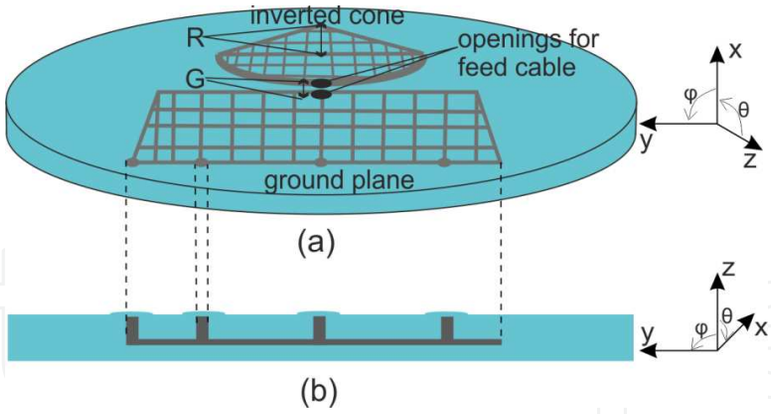

Figure 16. Schematic of the microfluidics- based stretchable ultra-wide band antenna: (a) overlook view and (b) cross view of microfluidic channels in a PDMS elastomer.

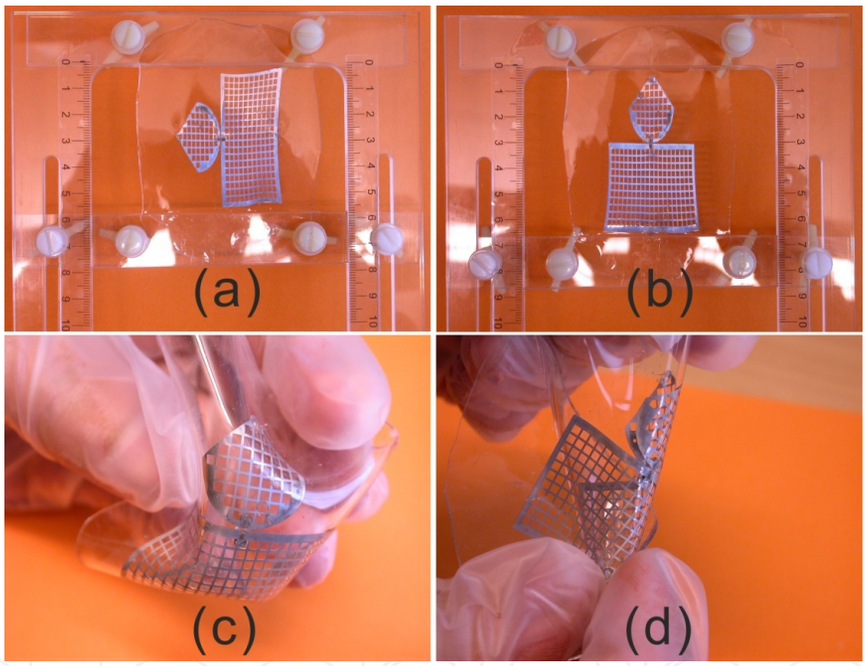

Figure 17. Photographs of the elastic PICA under deformation: (a) 40% strain along (a) *x*- and (b) *y*-axes, (c) and (d) severe folding and twisting. The coordinate system is shown in Figure 16.

Relative stretchability as high as 100% should be within reach according the data sheet of the PDMS elastomer in use. Openings in the top PDMS membrane as well as the rigid feed cable set an upper limit of approximately 50% on stretchability. Low temperature test is also performed, using a household freezer with a lowest temperature of –24 °C. No mechanical failure can be found after cooling the antenna prototype at –24 °C for 2 hours.

Port impedance and radiation characteristics of the microfluidics- based stretchable PICA are all measured at room temperature. Measured reflection coefficient, S_{11}, of the relaxed antenna is in line with the corresponding simulated result and good impedance matching (S_{11}<–10 dB) is achieved between 3 GHz and 11 GHz, as seen in Figure 18.

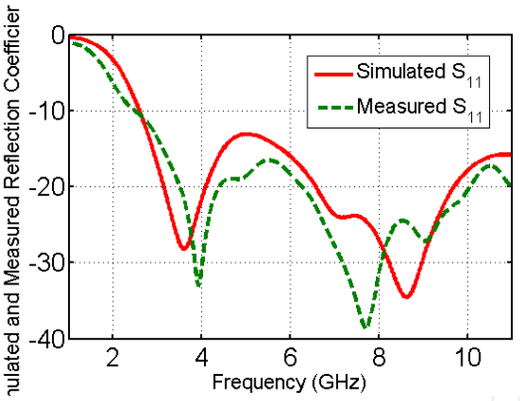

Figure 18. Simulated and measured S11 of the stretchable ultra-wide band PICA in its original state.

Reflection coefficients of the stretchable fluidic PICA are also characterized in various flexed states. Experimental data presented in Figure 19 indicate that robust impedance matching is achieved even if the microfluidic PICA is strained.

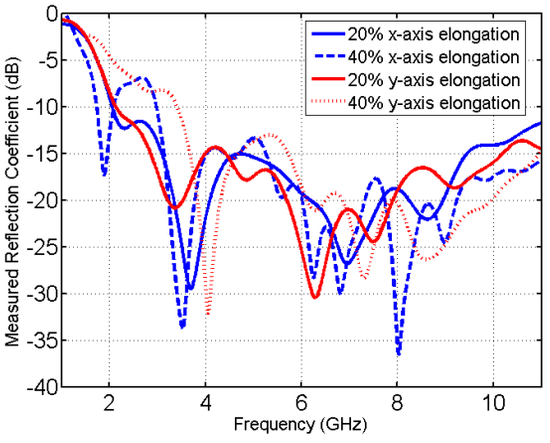

Figure 19. Measured S11 of the flexed PICA. The coordinate system can be found in Figure 16.

Stretching the antenna along its *x*-axis leads to increased height of the inverted cone and lowered first resonant frequency. Port impedance at higher frequencies remains stable in spite of stressing, as it is mainly governed by the impedance transformer formed by the tapered shape and the small gap between the antenna radiating element and the ground plane. Excessive strains along the *x*-axis might deteriorate impedance matching performance to some extent because of significantly increased gap size and severe deformation of the impedance transformer. Elongation along the *y*-axis only slightly impacts measured reflection coefficients because of relatively small changes in the tapered shape and the gap size. Radiation patterns of the relaxed and flexed elastic PICA are measured at 2.5 GHz and 5 GHz. Figure 20 illustrates the measured data at 2.5 GHz.

In comparison with antenna gain, variations on measured radiation patterns as a result of stressing are greater. Broad beam coverage similar to an ordinary monopole antenna is

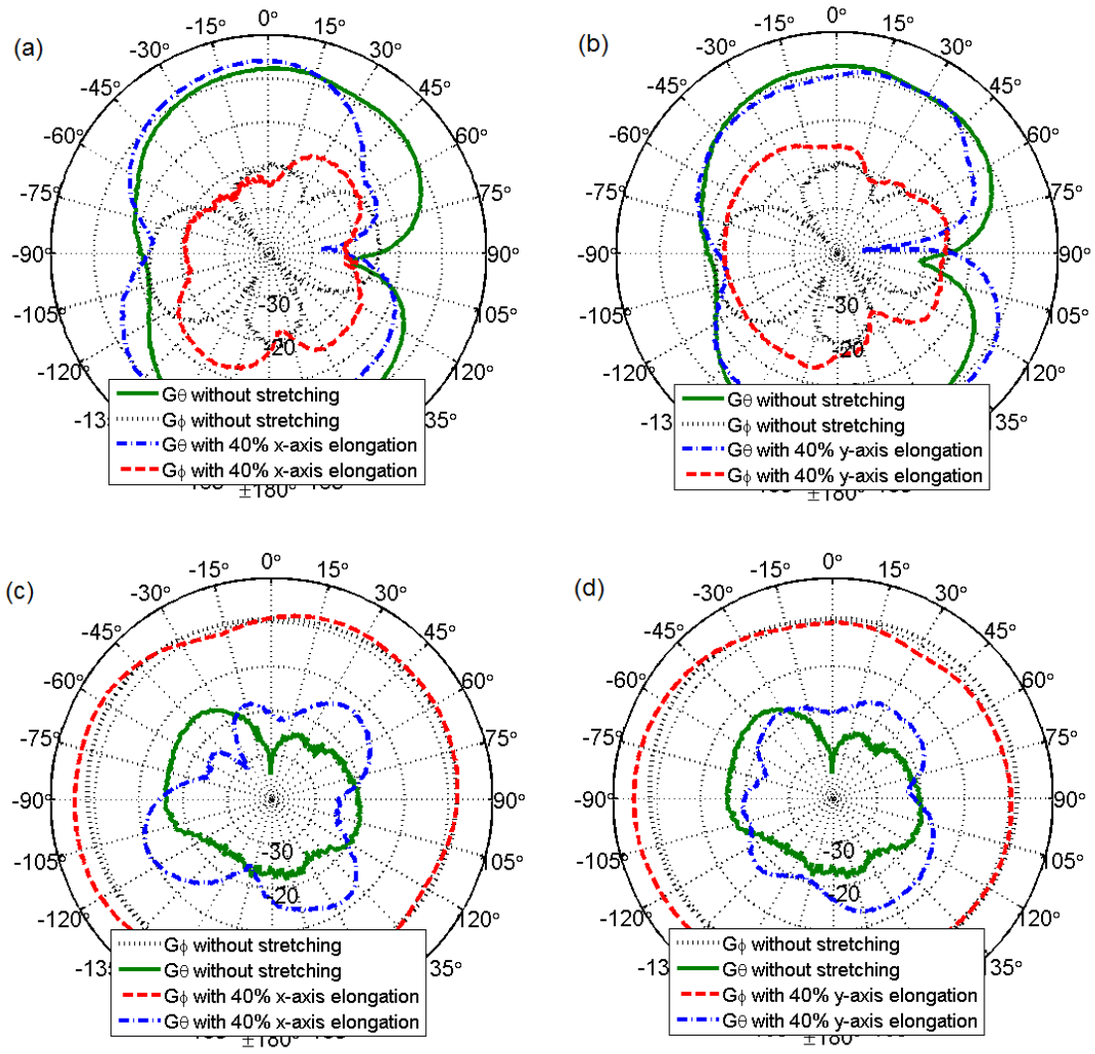

Figure 20. Measured radiation patterns of the relaxed and stressed PICA in the (a), (b) xz-, and (c), (d) yz-plane. The corresponding coordinate system is depicted in Figure 16.

achieved in both relaxed and flexed cases. Maximum gain of approximately 2.2 dBi is measured at 2.5 GHz. Detailed results on radiation characteristics of the resulting elastic PICA can be found in Cheng et al. [14]. Strong ripples are seen in measured radiation patterns at 5 GHz. The major cause for these fast ripples is frequency- dependent disturbance introduced by the feed cable in the experiments.

Radiation efficiency is another important figure of merit for terminal antennas featuring omnidirectional radiation patterns. A custom-designed reverberation chamber is employed for rapid radiation efficiency measurements. Experimental results at different frequencies are plotted in Figure 21.

Although measured radiation efficiency decreases a bit at 3 GHz during stretching, it still remains above 70%, an acceptable figure, better than many commercially available antennas. No significant efficiency drop is detected over the entire frequency range. This further verifies

http://dx.doi.org/10.5772/63376

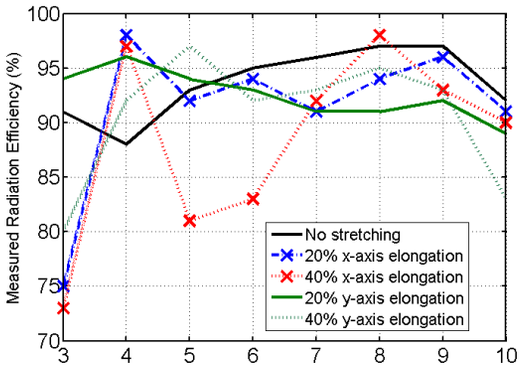

Figure 21. Measured radiation efficiency of the PICA in its relaxed and stretched states. The coordinate system is presented in Figure 16.

the robustness of electrical connections in the implemented PICA under different forms of deformation.

3.4. Multifunctional, microfluidics- based patch antenna and reversibly stretchable, self-contained, wireless strain sensor

A natural further step in the development of the emerging field of microfluidic soft electronics is to create more sophisticated multi-layered electronic devices and systems that can potentially open up a full spectrum of new applications. This, however, poses new challenges in device design, fabrication, and integration. The fabrication process of multi-layer microfluidic, elastomeric channels proposed in Section 2.2 is utilized to implement a reversibly stretchable, large-area, wireless strain sensor. This section details the design, fabrication, assembly, and characterizations of the sensor device.

The integrated wireless strain sensor contains an RF transmitter on a flexible PCB and a multifunctional, microfluidic, stretchable patch antenna for both wireless communication and strain sensing. The fluidic patch antenna is constructed in a double-layer configuration, *cf*. Figure 22. The principle for using an elastic antenna for strain sensing is simple. Because the resonant frequency of the patch antenna in use is largely determined by its electrical length along the x-axis, elongation along this direction would result in greater electrical length so that it decreases its resonant frequency. In the case of a patch antenna with narrow bandwidth (or high quality factor, Q), considerable impedance mismatch will occur at its original resonant frequency as a result of strain along its x-axis. When feeding such an antenna with a 50 Ω source at a constant power level, significantly decreased radiation will be measured in the far-field. Higher strain sensing sensitivity can be attained by reducing antenna bandwidth. But decreasing bandwidth would put high demands on fabrication precision. A tradeoff between sensitivity and fabrication yield has to be made. In addition to the multifunctional antenna, the integrated sensor also contains a simplified RF transmitter, which can be externally powered by a stack of two AA batteries connected serially. Details of this integrated electronic sensor device can be found in the schematic views presented in Figure 22.

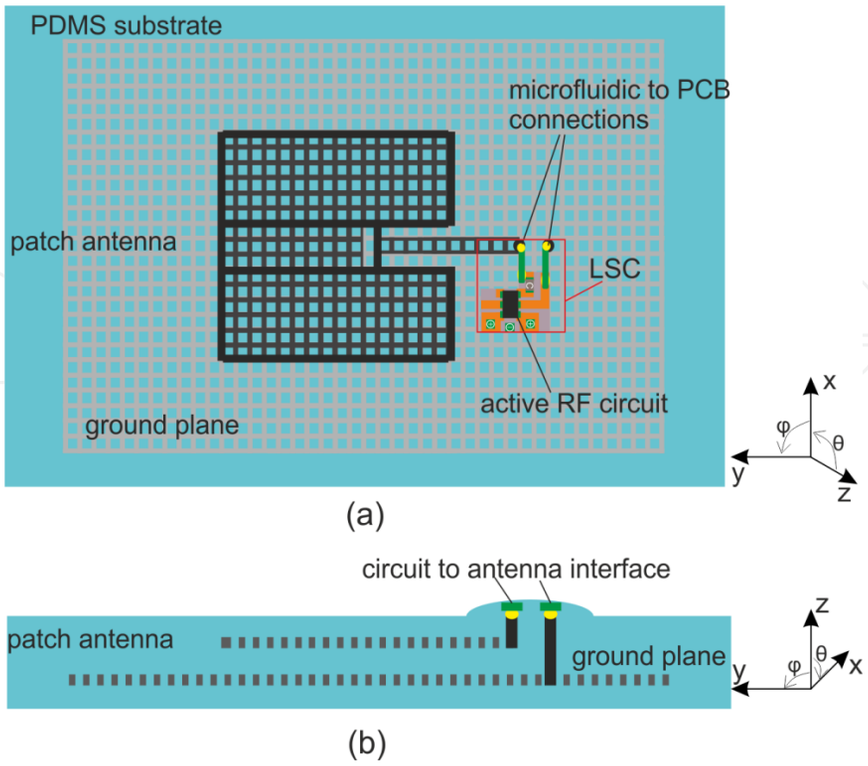

Figure 22. Schematic view of the proposed elastic wireless strain sensor: (a) top view and (b) cross view of microfluidic channels.

The designed patch antenna is fed by a short piece of microstrip. The spacing between the patch and the ground plane determines the bandwidth of the antenna. The greater the spacing is, the wider bandwidth the antenna features. Impedance bandwidth is also affected by dielectric losses of the substrate. Lossy dielectric materials would increase antenna bandwidth at the expense of radiation efficiency. Poor radiation efficiency should be definitely avoided, as it significantly shortens remote sensing range. Resembling microfluidic antennas reported in the previous sections, both the antenna patch and ground plane are realized in the meshed configuration. The active circuit assembled on a flex foil comprises a 1.5 GHz voltage controlled oscillator (VCO) associated with a few discrete components. The effective strain sensing area is as large as the overall size of the integrated sensor, approximately 110.0 mm × 80.0 mm. It makes the resulting wireless sensor well suited for remote, large-area strain sensing.

Mechanical properties should be taken into account in the design as well. Thinner PDMS substrates are preferred because of higher elasticity. A very thin substrate would, however, constrain the spacing between the patch and the ground plane, and lead to too narrow antenna bandwidth. Parametric analysis in numerical simulations shows that good compromise values for the overall thickness, and the spacing are 2.5 mm and 1.5 mm. A microfluidic, flexible, stretchable wireless strain sensor is implemented, following the fabrication and integration process described previously. Two openings on the top surface of the PDMS elastomer are utilized for hybrid integration with RF transmitter. A photograph of the fabricated sensor device is presented in Figure 23.

http://dx.doi.org/10.5772/63376

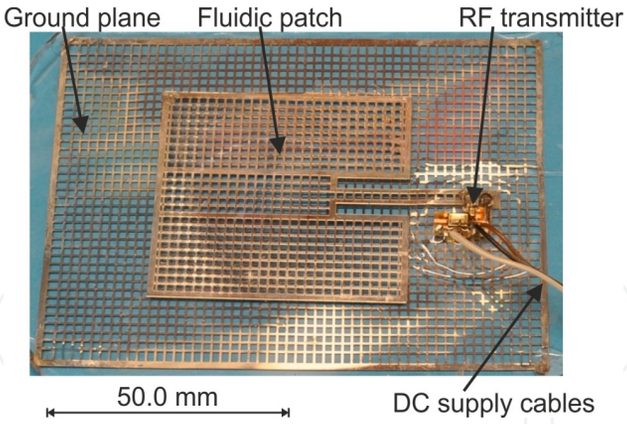

Figure 23. Photograph of the resulting microfluidics- based stretchable wireless strain sensor.

Prior to the final integration, the standalone patch antenna and RF transmitter circuit are tested individually. Reflection coefficients of the fluidic soft patch in response to varying strains are seen in Figure 24.

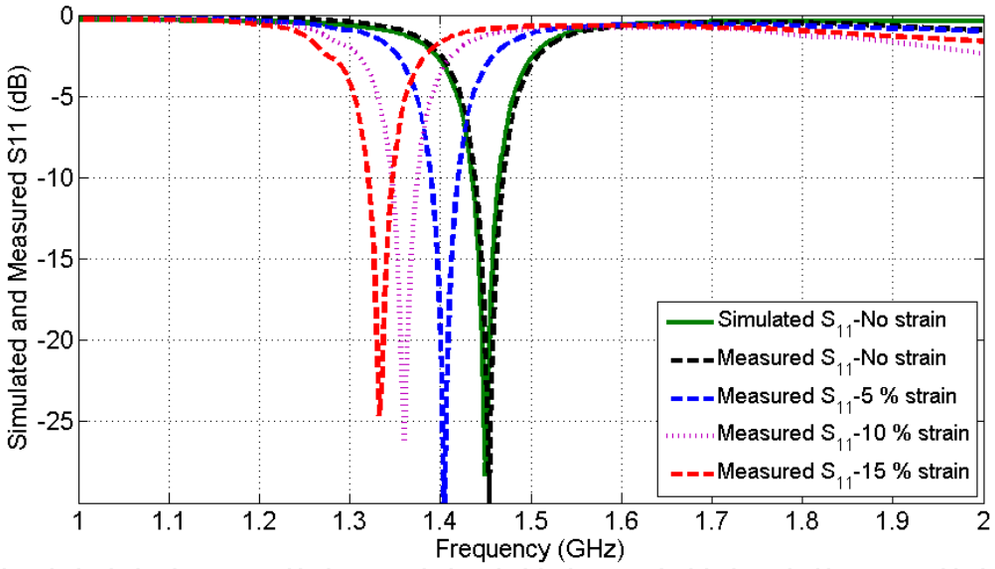

Figure 24. Simulated and measured S11 of the standalone fluidic patch antenna in its original state, and with varying strain along *x*-axis. The coordinate system is seen in Figure 22.

Experimental results indicate a dramatic resonant frequency decrease in response to incremental strain along the *x*-axis. Significant mismatch losses are observed at the oscillation frequency, 1.46 GHz, of the VCO during stretching. Measured radiation patterns (including mismatch losses) depicted in Figure 25 show greater than 10 dB realized antenna gain drop when the patch antenna is stressed from its original state to 15% elongation along the *x*-axis. Front-to-back ratio of radiation patterns is better than 10 dB. It should be noted that the meshed ground plane acts as an effective radiation shield and excellent front-to-back ratio of higher than 10 dB implies good forward radiation.

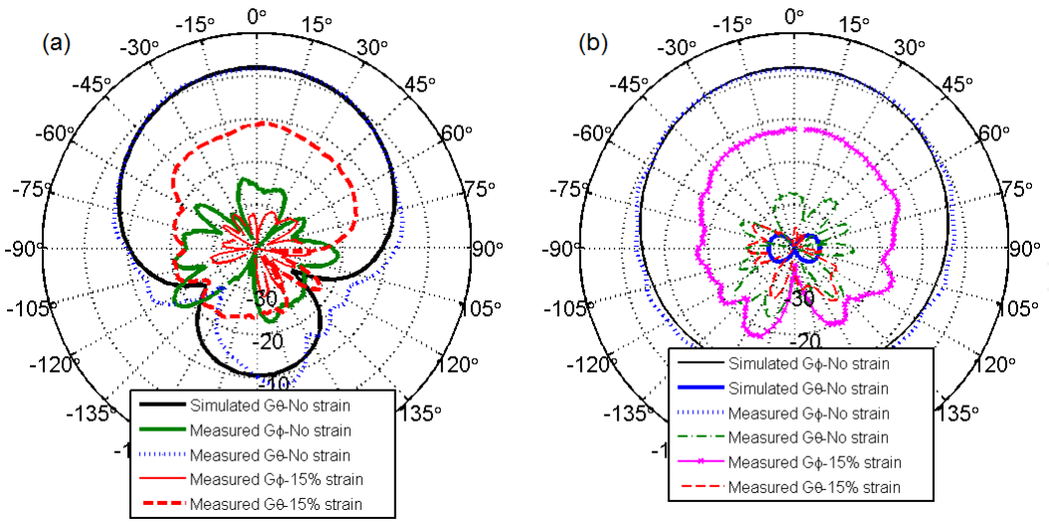

Figure 25. Simulated and measured radiation patterns (including mismatch losses) of the relaxed and flexed microfluidic patch antenna in the (a) xz- and (b) yz-plane. The coordinate system is shown in Figure 22.

After antenna measurements, the active circuit and the elastic antenna are heterogeneously integrated. On the other end of the wireless strain sensing system, a custom-designed receiver is developed to receive and interpret sensing data. The system diagram of the entire test setup for the elastic wireless strain sensor is illustrated in Figure 26.

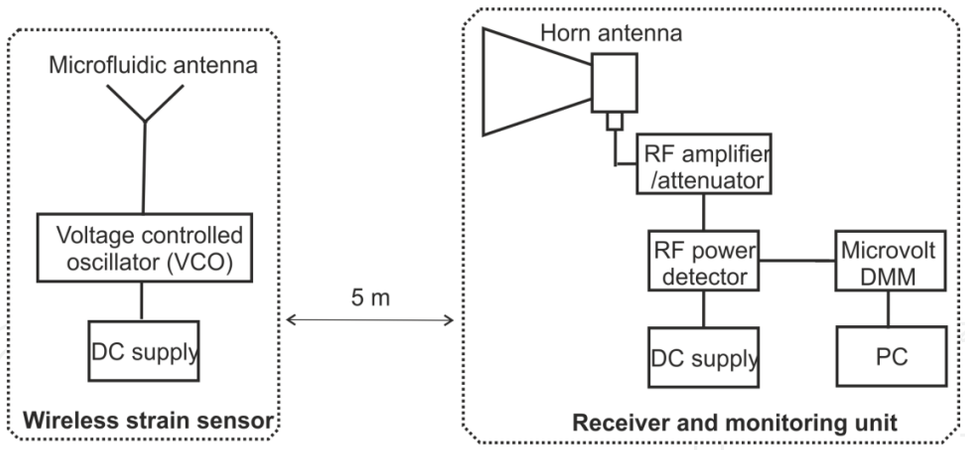

Figure 26. Illustration of the setup for demonstrating the microfluidic, reversibly stretchable, large-area wireless strain sensor.

As shown in Figure 26, the receiver consists of numerous sub-modules for RF power detection and is assisted by a personal computer (PC) for data readout and plotting. The output of the RF power detector is a DC voltage, proportional to the input RF power level. This voltage is measured by a high resolution digital multi-meter (DMM) controlled by the PC. The receiver unit is calibrated with varying RF power around 1.5 GHz, using a high precision synthesizer prior to the actual measurements.

http://dx.doi.org/10.5772/63376

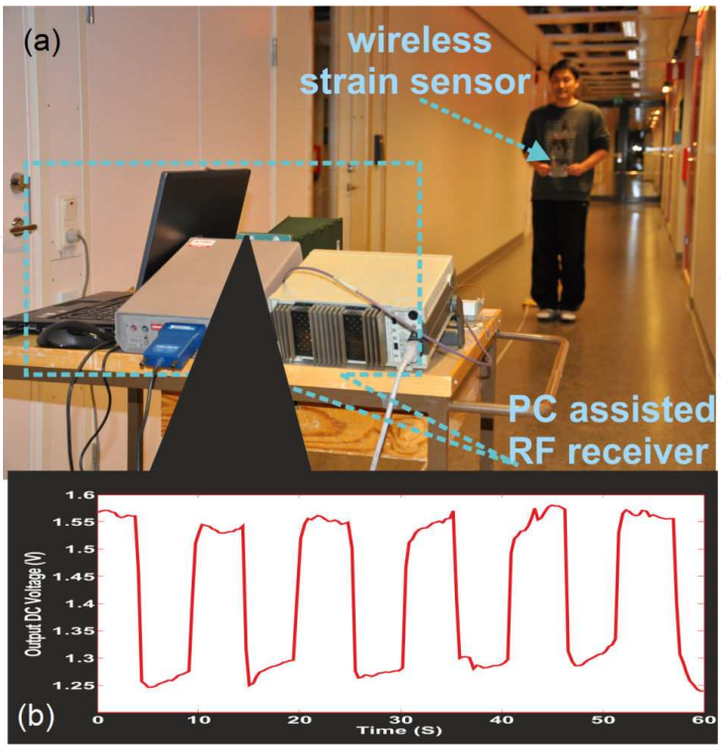

Figure 27. (a) Photograph of the demonstration of the elastic, wireless strain sensor. (b) Voltage readouts at a custom-designed PC-aided receiver.

The microfluidic, reversibly stretchable wireless strain sensor is tested in an ordinary office environment, *cf*. Figure 27. The distance between the integrated sensor and the receiver station is roughly 5 m. Repeated strain with a period of approximately 10 seconds is manually applied along the x-axis of the sensor. The plot in Figure 27 displays the data readout at the PC, which is in line with the manual stretch. Reversibility can also be clearly seen in the plot, as the measured voltage always returns to the original level after the removal of external strain. Such an integrated sensor can be deployed as a comfortable wearable electronic device for real-time monitoring of body motion.

4. Conclusion

An overview in the emerging field of ultracompliant, soft electronics that can be twisted, compressed, and stressed into almost any arbitrary shapes has been presented. Different strategies for realizing bendable, flexible, stretchable electronic devices and systems have been briefly discussed. Microfluidics- based soft electronics, one of the most promising approaches for implemented elastomeric electronics, has been addressed in detail. Fabrication techniques, hybrid integration concepts, as well as various electronic devices built in microfluidic, elastic formats are the focus of this chapter. Appealing application examples, ranging from single-layer standalone fluidic stretchable antennas to multi-layer, self-contained, large-area, wireless sensors, have been demonstrated.

Research efforts in incorporating new materials and novel technologies into soft electronics are ongoing. Figure 28 shows an example of a hand-shaped, soft, rubbery sensor for multi-point, remote pressure sensing. Emerging nanomaterials and fabrication processes, e.g., pressure-activated conductive rubber and inkjet-printed graphene -based flexible circuits, are introduced to create novel pressure sensors and active RF electronics. Feasibilities of implementing microfluidic, elastic EM energy harvesting devices are also being explored. Successful outcomes will pave the way for realizing batteryless, ultracompliant, wearable and implanted electronics that can be powered by ambient EM energy generated from billions of wireless devices around us.

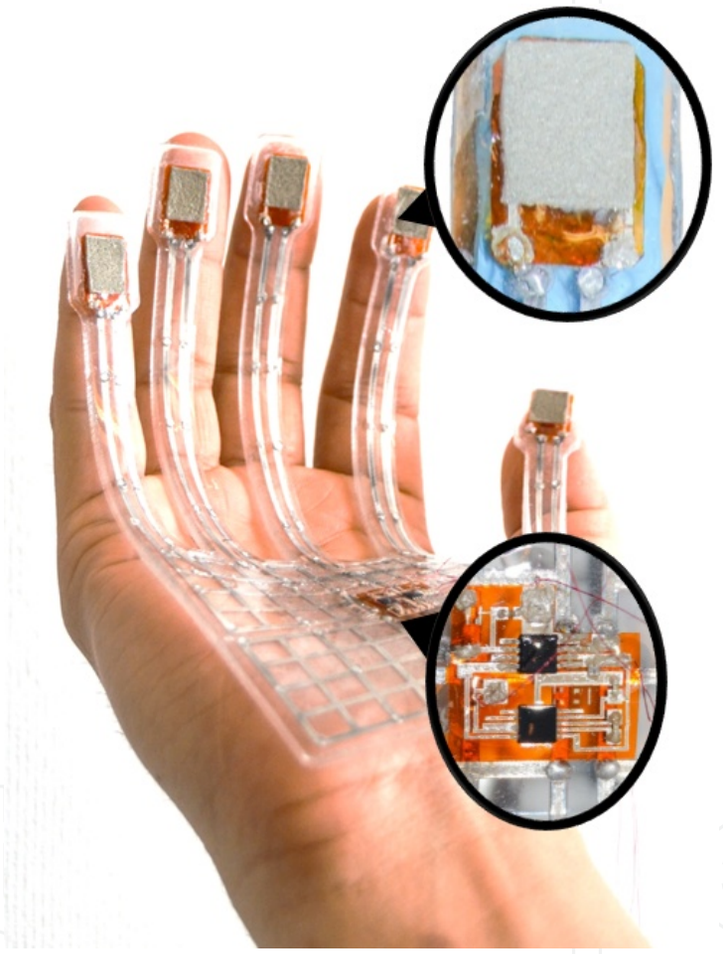

Figure 28. Photograph of the stretchable multi-point, wireless pressure sensor prototype.

Microfluidic flexible, compressible, stretchable electronics together with other members in the new category of soft electronics are reshaping the world of electronics so as to the future of our daily life. The number of cell phones already outpaced the world population in 2014. It is anticipated that the total number of connected devices will grow to approximately seven times of the entire population in the coming 5 years, among which billions of soft electronic devices will be found in many new applications, including healthcare/medical monitoring, tissue engineering, bio-inspired robotics, and so on.

Acknowledgements

Dr. Shi Cheng currently holds a Young Research Fellow position financed by the Swedish Research Council (VR) under the contract (Avtals-ID: C0486501). Also Dr. Jiantong Li acknowledges Göran Gustafsson Foundation for the financial support through the Young Researcher Prize (No. 1415 B).

Author details

Babak Taghavi[1], Jiantong Li[1], Mikael Östling[1] and Shi Cheng[1,2]

1 KTH, Royal Institute of Technology, Sweden

2 Ericsson AB, Sweden

References

[1] Rutherford J.J.Wearable Technology. Engineering in Medicine and Biology Magazine, IEEE. 2010;29(3):19-24. DOI: 10.1109/MEMB.2010.936550

[2] Vertechy R., Accoto D. Wearable Robotics. Robotics & Automation Magazine, IEEE. 2014;21(4):19-110. DOI: 10.1109/MRA.2014.2364732

[3] Honda W., Harada S., Arie T., Akita S., Takei K. Flexible Electronics: Wearable, Human-Interactive, Health-Monitoring, Wireless Devices Fabricated by Macroscale Printing Techniques. Advanced Functional Materials. 2014;24(22):3298. DOI: 10.1002/adfm.201470144

[4] Rogers J.A., Someya T., Huang Y. Materials and Mechanics for Stretchable Electronics. Science. 2010;327:1603. DOI: 10.1126/science.1182383

[5] Kim D.H., Ahn J.H., Choi W. M., Kim H.S., Kim T.H., Song J. Z., et al.. Stretchable and Foldable Silicon Integrated Circuits. Science. 2008;320(5875):507-511. DOI: 10.1126/science.1154367

[6] Lacour S.P., Wagner S., Huang Z.Y., Suo Z. Stretchable Gold Conductors on Elastomeric Substrates. Applied Physics Letters. 2003;82(15):2404-2406. DOI: 10.1063/1.1565683

[7] Lacour S. P., Jones J., Wagner S., Li T., Suo Z. Stretchable Interconnects for Elastic Electronic Surfaces. Proceedings of the IEEE. 2005;93(8):1459 -1467. DOI: 10.1109/JPROC.2005.851502

[8] Haopeng W., Debao Z., Jianguo C. Development of a Stretchable Conductor Array with Embedded Metal Nanowires. IEEE Transactions on Nanotechnology. 2013;12(4):561 -565. DOI: 10.1109/TNANO.2013.2258172

[9] Brosteaux D., Axisa F., Gonzalez M., Vanfleteren J. Design and Fabrication of Elastic Interconnections for Stretchable Electronic Circuits. Electron Device Letters, IEEE. 2007;28(7):552 - 554. DOI: 10.1109/LED.2007.897887

[10] Siegel A. C., Bruzewicz D. A., Weibel D. B., Whitesides G. M. Microsolidics: Fabrication of Three-Dimensional Metallic Microstructures in Poly(dimethylsiloxane). Advanced Materials. 2007;19:727–733. DOI: 10.1002/adma.200601787

[11] Kim H., Son C., Ziaie B. A Multiaxial Stretchable Interconnect Using Liquid-Alloy-Filled Elastomeric Microchannels. Applied Physics Letters. 2008;92(011904):1-3. DOI: 10.1063/1.2829595

[12] Dickey M. D., Chiechi R. C., Larsen R. J., Weiss E. A., Weitz D. A., Whitesides G. M. Eutectic Gallium-Indium (EGaIn): A Liquid Metal Alloy for the Formation of Stable Structures in Microchannels at Room Temperature. Advanced Functional Materials. 2008;18:1097-1104. DOI: 10.1002/adfm.200701216

[13] Cheng S., Rydberg A., Hjort K., Wu Z. Liquid Metal Stretchable Unbalanced Loop Antenna. Applied Physics Letters. 2009; 94:144103. DOI: 10.1063/1.3114381

[14] Cheng S., Wu Z., Hallbjörner P., Hjort K., Rydberg A. Foldable and Stretchable Liquid Metal Planar Inverted Cone Antenna. IEEE Transactions on Antennas and Propagation. 2009;57(12):3765-3771. DOI: 10.1109/TAP.2009.2024560

[15] Kubo M., Li X., Kim C., Hashimoto M., Wiley B. J., Whitesides G.M. Stretchable Microfluidic Radiofrequency Antennas. Advanced Materials. 2010;22:2749-2752. DOI: 10.1002/adma.200904201

[16] Cheng S., Wu Z. Microfluidic Stretchable RF Electronics. Lab on a Chip. 2010;10:3227-3234. DOI: 10.1039/c005159d

[17] Cheng S., Wu Z. A Microfluidic, Reversibly Stretchable, Large-Area Wireless Strain Sensor. Advanced Functional Materials. 2011;21:2282–2290. DOI: 10.1002/adfm.201002508

[18] Hayes G. J., So J. H., Qusba A., Dickey M. D., Lazzi G. Flexible Liquid Metal Alloy (EGaIn) Microstrip Patch Antenna. IEEE Transactions on Antennas and Propagation. 2012;60(5):2151-2156. DOI: 10.1109/TAP.2012.2189698

[19] Huang Y., Wang Y., Xiao L., Liu H., Dong W., Yin Z. Microfluidic Serpentine Antennas with Designed Mechanical Tunability. Lab on a Chip. 2014;14:4205-4212. DOI: 10.1039/c4lc00762j

[20] Jeong S. H., Hagman A., Hjort K., Jobs M., Sundqvist J., Wu Z. Liquid Alloy Printing of Microfluidic Stretchable Electronics. Lab on a Chip. 2012;12:4657-4664. DOI: 10.1039/c2lc40628d